Inorganic Chemistry

Article

pubs.acs.org/IC

Electrocatalytic Proton Reduction by Dimeric Nickel Complex of a Sterically Demanding Pincer-type NS_2 Aminobis(thiophenolate) Ligand

Alexander Mondragón,[†] Marcos Flores-Alamo,[‡] Paulina R. Martínez-Alanis,[†] Gabriel Aullón,[§] Víctor M. Ugalde-Saldívar,[‡] and Ivan Castillo*,[†]

[†]Instituto de Química and [‡]Facultad de Química, Universidad Nacional Autónoma de Mexico, Circuito Exterior, CU, Ciudad de México, DF, 04510, México

[§]Departament de Química Inorgànica and Institut de Química Teòrica i Computacional, Universitat de Barcelona, Martí i Franquès 1-11, 08028 Barcelona, Spain

Supporting Information

ABSTRACT: Basic methanolysis of a sterically hindered aminobis(*S*-arylthiocarbamate) affords a novel aminobis(thiophenolate) pincer-type ligand NS_2^{2-}; the in situ generated dianion reacts cleanly with Ni^{2+} and Zn^{2+} resulting in dimeric complexes with bridging thiophenolate ligands, as determined spectroscopically and by X-ray crystallography. The C_2-symmetric $[Ni(NS_2)]_2$ dimer (**1**) has a square planar coordination geometry around the Ni^{2+} ions, while the $[Zn(NS_2)]_2$ analogue (**2**) is characterized by a distorted tetrahedral geometry around each independent Zn^{2+} ion. Addition of the neutral monodentate donor L = 2,6-xylylisocyanide to $[Ni(NS_2)]_2$ affords the monomeric complex $[LNi(NS_2)]$ (**3**), which is characterized in the solid state by a square planar geometry with the isocyanide donor trans to the tertiary amine of NS_2. The pincer NS_2 ligand provides redox plasticity to **1**, manifested in the accessibility of the putative $Ni^{+}Ni^{+}$ and $Ni^{3+}Ni^{3+}$ dimeric complexes, based on comparative cyclic voltammetry studies with **2** and **3**. The redox properties of **1** endow it with hydrogenase-type activity, as evidenced in the electrocatalytic reduction of protons in a mixed aqueous/organic phase, as well as the oxidation of hydrides from $NaBH(OAc)_3$. Both **1** and **3** are resilient under protic and oxidative conditions, as evidenced in reactivity tests monitored by UV−vis spectroscopy.

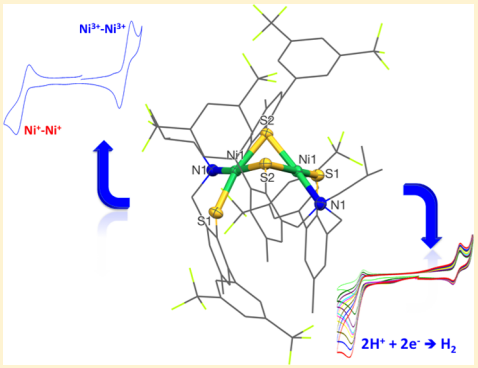

INTRODUCTION

Nickel has emerged as an essential trace element in living systems, participating in redox reactions with the aid of thiolate ancillary ligands provided by cysteine residues. To gain a better understanding of how the sulfur-rich environment facilitates such redox transformations, considerable efforts have been devoted to the development of sulfur-rich model systems akin to, for example, the active sites of [NiFe] hydrogenases[1] and nickel-dependent carbon monoxide dehydrogenase/acetyl coenzyme A synthase.[2] Both metalloenzymes require a certain degree of electronic plasticity to access a variety of redox states for the nickel centers involved. Chelating and tunable thiol-based ligands are thus appealing synthetic targets for the development of metal complexes inspired by the active sites of such enzymes.[3,4] Although several types of sulfur-containing chelating ligands have been reported, the area of tridentate NS_2 (pincer-type) donors is dominated by synthetically accessible thioethers and thioamides.[5] The corresponding thiolate or thiophenolate ligands are characterized by a rigid framework with limited steric protection, leading to aggregation, and high sensitivity toward oxidation.[6,7]

In this context, we adapted a synthetic route described originally for the preparation of relatively hindered ortho-substituted amiotrithiophenols from commercial salicylaldehydes.[8] We thus developed the key precursor 2-formyl-4-methyl-6-[3,5-bis(trifluoromethyl)phenyl]-*S*-phenyl thiocarbamate (Scheme 1c), which offers a 2-fold advantage relative to previous reports: (i) the electron-withdrawing nature of the bis(trifluoromethyl)phenyl substituent ortho to the thiocarbamate moiety, resulting in better yields during thermal conversion by the Newman−Kwart rearrangement (NKR) of the *O*- to the *S*-thiocarbamate, (ii) the electron-withdrawing groups additionally render the sulfur donors less susceptible to oxidation by air, and (iii) the increased steric bulk of such ortho substituents may prevent uncontrolled assembly of polymeric or oligomeric sulfur-bridged metal complexes. The first consideration allowed us to obtain the bis(*S*-arylthiocarbamate)amine ligand precursor (Scheme 1D) in an overall yield of 51% from the substituted salicylaldehydes.[9]

Received: October 23, 2014
Published: December 24, 2014

DOI: 10.1021/ic502547y
Inorg. Chem. 2015, 54, 619−627

Scheme 1. Synthesis of Pincer-type NS_2 Ligand[a]

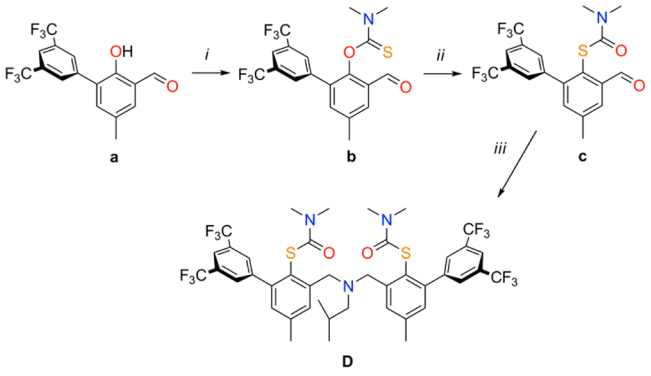

[a](i) DMAP, Cl(CS)NMe_2, DME, 18 h, 80 °C; (ii) NMP/230 °C; (iii) $NaBH(OAc)_3$, ^{t}BuNH_2, THF/r.t., overnight.

We herein present the synthesis and characterization of Ni^{2+} and Zn^{2+} complexes with the dianionic NS_2 pincer ligand obtained from **D**, which imparts geometric flexibility due to the methylene connectors between the central amine and the thiophenol groups. As mentioned above, they are sterically hindered due to the ortho substituents relative to the sulfur donors in the thiophenols and may also prevent oxidation by removing electron density from the thiophenolate donors. This makes them suitable ligands for the exploration of the electronic and catalytic properties of the earth-abundant Ni complexes with potential impact in energy storage.[10]

RESULTS AND DISCUSSION

Access to the pincer-type ligand employed NS_2 involves the NKR of an *o*-formyl-*O*-arylthiocarbamate (**b**) using *N*-methylpyrrolidinone (NMP) as solvent to obtain the key precursor 2-formyl-4-methyl-6-(3,5-bis(trifluoromethyl)-phenyl)-*S*-phenylthiocarbamate (**c**) as building block (Scheme 1).[9] This *S*-arylthiocarbamate **c** was subjected to reductive amination conditions with isobutylamine, affording the bis(*S*-arytiocarbamate)amine ligand precursor (**D**). The latter compound **D** was deprotected with sodium methoxide in tetrahydrofuran (THF) under an inert atmosphere, followed by addition of solid $NiCl_2{\cdot}6H_2O$ or $ZnCl_2$ to a solution of the in situ generated dithiolate amine NS_2^{2-}, affording the corresponding Ni^{2+} and Zn^{2+} complexes. In the case of nickel complex, the yellow solution of the NS_2 ligand changed color to very dark green immediately after addition of $NiCl_2{\cdot}6H_2O$ (Scheme 2). For the zinc complex there was no noticeable change after the metalation reaction, except for the formation of a colorless precipitate after stirring for 2 h.

Scheme 2. Synthesis of Ni^{2+} (1) and Zn^{2+} (2) Complexes of NS_2[a]

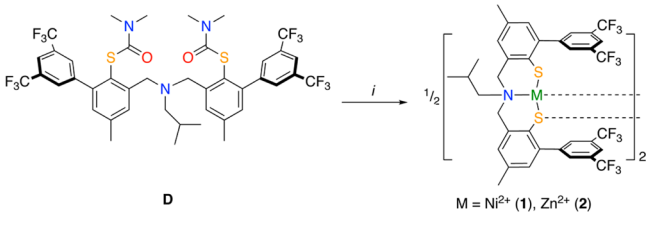

[a](i) MeONa, THF, 4 d, 60 °C, then $NiCl_2{\cdot}6H_2O$ or $ZnCl_2$, r.t., 2 h.

Both complexes were isolated as crystalline solids after filtration and removal of solvents. In the case of the Ni complex the dark green solid obtained was recrystallized from a 7:3 diethyl ether/CH_3CN solution. Complex **1** was initially analyzed by ^{1}H NMR spectroscopy, revealing the disappearance of the signals corresponding to thiocarbamate moiety at δ 2.87 ppm; additionally, the diastereotopic protons of the methylene group in the ^{t}Bu fragment split into two doublets relative to the parent *S*-thiocarbamate. The signals corresponding to the ^{t}Bu-methyl group shift downfield (δ 1.58 ppm) and upfield (δ 0.76 ppm) with respect to the signals in the free ligand (δ 0.97 ppm, see Supporting Information Figure S1). In the case of compound **2**, colorless crystals were obtained by slow evaporation of a 7:3 diethyl ether/CH_3CN mixture. The disappearance of the carbamate group resonances was also evidenced by ^{1}H NMR spectroscopy as well as by the displacement of the signals corresponding to the equivalent ^{t}Bu-methyl groups (Supporting Information, Figure S5).

Fast atom bombardment mass spectrometry (FAB-MS) shows a peak at *m*/*z* 1652 (Supporting Information, Figure S3), corresponding to exactly double the molecular weight of the putative $[Ni(NS_2)]$ expected for a 1:1 stoichiometry; the above evidence led us to propose a dimeric nature for complex **1**, $[Ni(NS_2)]_2$. Likewise, mass spectrometric analysis of the Zn^{2+} complex **2** exhibits a pattern similar to that observed for **1**. In this case a peak was detected at *m*/*z* 1664 (Supporting Information, Figure S7), also corresponding to exactly twice the mass of the monomeric complex $[Zn(NS_2)]$ (expected *m*/*z* 832); thus, a dimeric structure was also postulated for **2**, $[Zn(NS_2)]_2$. These formulations were confirmed unambiguously by structural characterization of both complexes.

Structural Analysis. Complex **1** crystallizes in the monoclinic space group *C*2/*c*; the geometry is best described as a slightly distorted square planar around the Ni^{2+} ions, which are related by a crystallographic C_2 axis. Each Ni^{2+} is coordinated by two sulfur atoms of the pincer-type ligand, and the nitrogen atom of the tertiary amine; this is complemented by a bridging sulfur atom of another monomeric unit located trans to the N atom, giving rise to the observed dimeric structure (Figure 1). For each metal center, the trans S−Ni−S angle is 164.21(4)°, whereas the trans N−Ni−S angle is 169.34(9)°. As mentioned above, the two square planes around the Ni ions, defined by N1, S1, S2, and the symmetry-related S2*, are joined along one edge by means of S2 and S2* (see Table 1); thus, each monomeric unit has a nonbridging thiolate ligand that may be considered electron-rich.[7b,d] The coordination planes are at an angle of 85.37(3)°, with the Ni ions at a distance of 2.7016(8) Å (Table 1 and Figure 1). Despite the steric hindrance imparted by the NS_2 ligand, a bent endo conformation of the thiolate groups is expected for chelate ligands according to previous theoretical and structural analyses.[11] Dimer formation with related ligands has previously been reported,[7] although the cases of NS_2 donor sets are limited to aliphatic systems. In such cases, solid-state characterization of the Ni^{2+} complexes obtained has also revealed bridging thiolates between the nickel ions.[7a,b,d,e]

Complex **1** reproduces closely structural parameters of the oxidized form of the A-cluster (A_{ox}), the dinuclear ($Ni^{2+}Ni^{2+}$) portion of acetyl-CoA-synthase/CO-dehydrogenase.[2,12] Despite the fact that **1** is a homodimeric complex, the Ni−Ni distance of 2.7016 Å may additionally be relevant from a functional perspective for a potential hydrogenase activity (see

DOI: 10.1021/ic502547y
Inorg. Chem. 2015, 54, 619−627

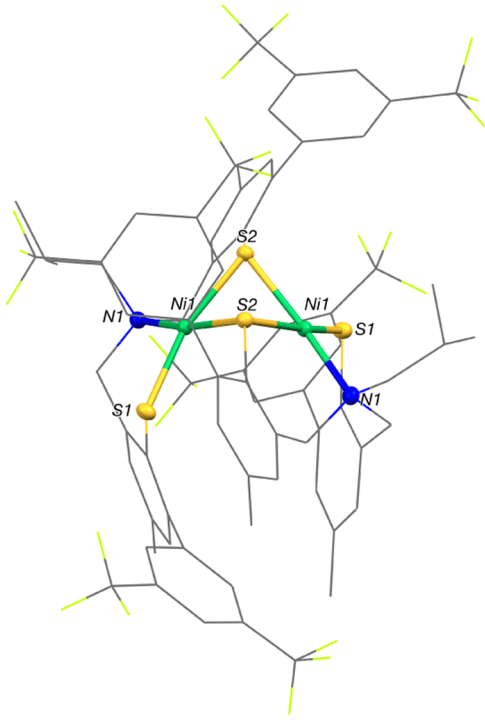

Figure 1. Mercury diagram of complex **1**. H and minor-occupancy atoms are omitted, and C and F atoms are shown as wireframe for clarity; color code: C, gray; F, lime; S, yellow; N, blue; Ni, green.

Table 1. Selected Bond Distances (Å) and Bond Angles (deg) for $[Ni(NS_2)]_2$ 1 and $[Zn(NS_2)]_2$ 2

		1	
Ni1–Ni1*	2.701(8)	S1–Ni1–S2	164.2(4)
Ni1–S1	2.205(1)	S2*–Ni1–N1	169.34(9)
Ni1–S2	2.204(1)	S1–Ni1–N1	97.69.4(9)
Ni1–S2*	2.213(1)	S2–Ni1–N1	95.37(9)
Ni1–N1	1.980(3)	Ni1–S1*–Ni1*	77.42(3)
		2	
Zn1–Zn2	3.070(5)	S3–Zn1–S2	115.74(3)
Zn1–S3	2.225(7)	S1–Zn1–N1	118.19(7)
Zn1–S2	2.391(9)	S3–Zn1–S1	127.55(3)
Zn1–S1	2.400(7)	S1–Zn1–S2	96.57(3)
Zn1–N1	2.087(2)	Zn1–S1–Zn2	77.69(2)
Zn2–S4	2.223(7)	S1–Zn2–N2	102.10(7)
Zn2–S2	2.322(6)	S4–Zn2–S1	120.56(3)
Zn2–S1	2.393(9)	S1–Zn2–S2	98.63(3)
Zn2–N2	2.047(2)	Zn1–S2–Zn2	79.26(2)

below), since Ni–Fe distances within the range of 2.5–2.9 Å have been determined for [NiFe]ases.[1,13]

As we expected, the coordination geometry is quite different around the Zn^{2+} ions in **2** (Table 1). Each crystallographically independent Zn center is in a distorted tetrahedral environment, and as in the case of **1**, each Zn^{2+} ion reaches a coordination number of four with a sulfur atom bridging two metal centers of the dimeric structure observed (Figure 2). The solid-state structure of **2** is less symmetric than that of **1**, so that each tridentate NS_2 ligand in **2** has a different structural arrangement; therefore, the S1–Zn2–S4 angle is 120.56(3)°, while the S2–Zn2–S3 angle is 115.74(3)°. In addition, the planes defined by N1–Zn1–S3 and S4–Zn2–N2 are joined along one edge by the bridging S1 and S2 atoms. The planes

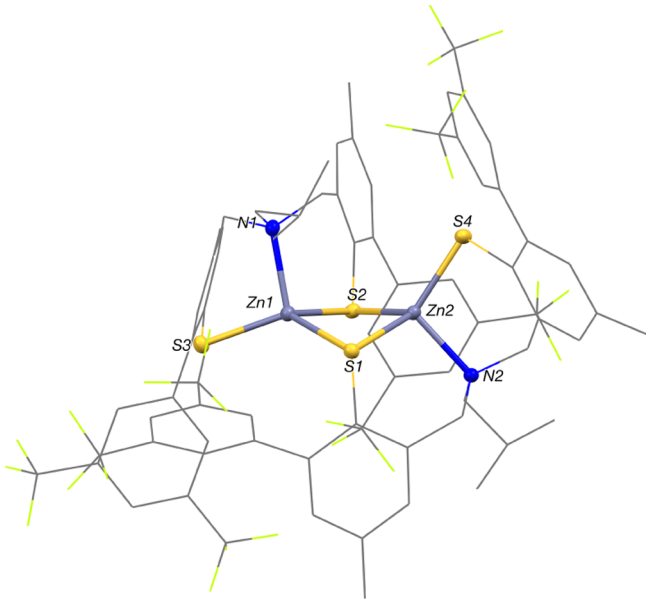

Figure 2. Mercury diagram of complex **2**. H and minor-occupancy atoms are omitted, and C and F atoms are shown as wireframe for clarity; color code: Zn, lilac.

defined by S1–Zn1–S2 and S1–Zn2–S2 are at a dihedral angle of 148(3)° (85.37° in **1**), and with the Zn^{2+} ions at a distance of 3.070(5) Å (see Table 1). Overall, the deviation from ideal tetrahedral coordination geometry may be attributed to the relatively constrained nature of the pincer NS_2^{2-} ligand, which appears to favor square planar coordination geometries.

In related dimeric Ni^{2+} complexes, the reactions with a variety of anionic ligands, including CN^-,[7b] RS^-, OH^-, and ArS^-,[7c] result in the corresponding monomers. In the case of **1**, addition of PPh_3, OH^-, or CN^- did not lead to any changes in the dimeric compound, even if the reactions were carried out at reflux temperature in THF. Nonetheless, the reaction with 2 equivs of the neutral ligand CNXyl (CNXyl = 2,6-dimethylphenylisocyanide) in THF solution resulted in an immediate color change from dark green to reddish brown (Scheme 3). ^1H NMR spectra of this new compound

Scheme 3. Synthesis of Monomeric Complex 3[a]

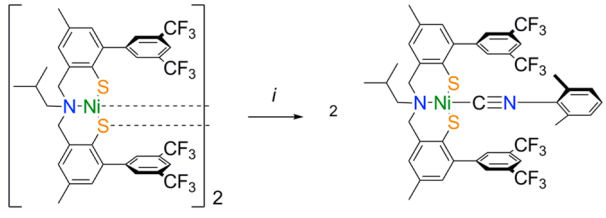

1 **3**

[a](i) THF, 2 equiv of (2,6-$Me_2C_6H_3CN$), r.t., 8 h.

$[(XylNC)Ni(NS_2)]$ **3** (Supporting Information, Figure S8) shows that the aliphatic protons of the ^{t}Bu group appear as a single set of resonances; additionally, a new singlet at δ 1.83 ppm integrating to 6H was assigned to the methyl groups on the 2 and 6 aromatic positions of the isocyanide, thus confirming the presence of the exogenous ligand coordinated to the Ni^{2+} center.

DOI: 10.1021/ic502547y
Inorg. Chem. 2015, 54, 619–627

Complex **3** allowed us to gauge the capability of the $(NS_2)Ni$ fragment to donate electron density by means of backdonation to the isocyanide ligand, as judged by FT-IR spectroscopy. The corresponding ν(CN) band is present at 2166 cm^{-1} (Supporting Information, Figure S11), compared to 2123 cm^{-1} for the free isocyanide. Although there is not a significant degree of backbonding from the metal center to the π^* orbital of the isocyanide, the high oxidation state of the nickel ion is likely responsible for this observation. Despite the fact that **3** has a relatively high ν(CN) frequency, complexes with related ancillary ligands give rise to even higher stretching frequencies (and less backdonation), with ν(CN) values at 2181 cm^{-1},[14a] 2192 cm^{-1},[14b] and 2196 cm^{-1},[14c] so that the $(NS_2)Ni$ moiety can be considered electron-rich among analogous Ni^{2+} complexes.

X-ray quality crystals of **3** were obtained by slow evaporation of a concentrated 4:1 THF/CH_3CN solution. As expected, the isocyanide ligand coordinates trans to the central amine donor, giving rise to a monomeric square planar complex (Figure 3).

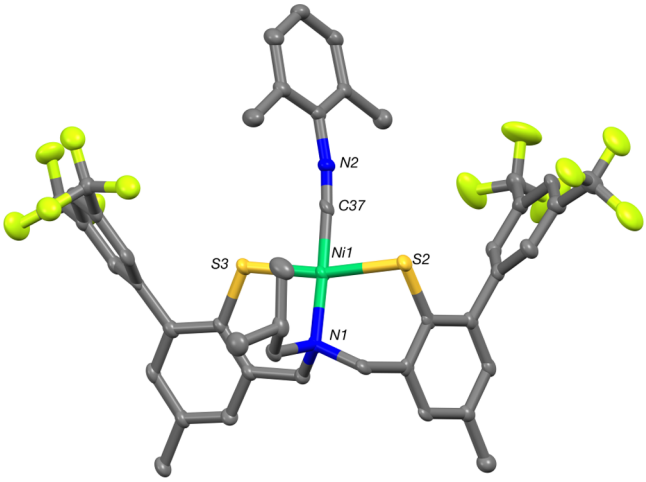

Figure 3. Mercury diagram of **3**: H and minor-occupancy atoms are omitted for clarity; color code: C, gray; F, lime; S, yellow; N, blue; Ni, green.

The Ni^{2+} ion is essentially within the plane (0.01%) defined by the S3, N1, S2, and C37 donor atoms (Table 2 and Figure 3).

Table 2. Selected Bond Distances (Å) and Bond Angles (deg) for [(XylNC)Ni(NS2)] 3

Ni1−S3	2.187(1)	S3−Ni1−S2	167.8(6)
Ni1−S2	2.224(1)	N1−Ni1−C37	177.8(2)
Ni1−C37	1.805(4)	Ni1−C37−N2	176.0(4)
Ni1−N1	1.972(3)	S3−Ni1−N1	94.4(1)

The planarity around the nickel center in **3** appears to be accommodated by the flexibility of the ligand, since the methylene bridges between the aromatic groups and the nitrogen atom are located above and below the plane, thus relieving the congestion imposed by the bulky substituents ortho to the sulfur donors. The aromatic fragment of the 2,6-dimethylphenylisocyanide ligand is at an angle of 62.05(1)° with respect to the square plane around Ni^{2+}.

Optical Spectroscopy. UV−vis spectra of sulfur-containing transition-metal complexes provide useful information regarding the nature of the M−S bonds present; for example, the intensity of the absorption bands, as well as their frequencies, reflect the degree of covalency of the bonds.[15] The electronic absorption spectrum of complex **1** exhibits bands at 235 (ε = 50 638 M^{-1} cm^{-1}, intra L → L), 260 (ε = 27 676 M^{-1} cm^{-1}, shoulder inter L → L), 310 (ε = 20 088 M^{-1} cm^{-1}, S → Ni), 361 (ε = 17 640 M^{-1} cm^{-1}, S → Ni), 422 (ε = 7428 M^{-1} cm^{-1}, shoulder S* → Ni), and 647 nm (ε = 1385 M^{-1} cm^{-1}, d−d band)[7f] (Figure 4, blue line). The band at 235 nm was assigned

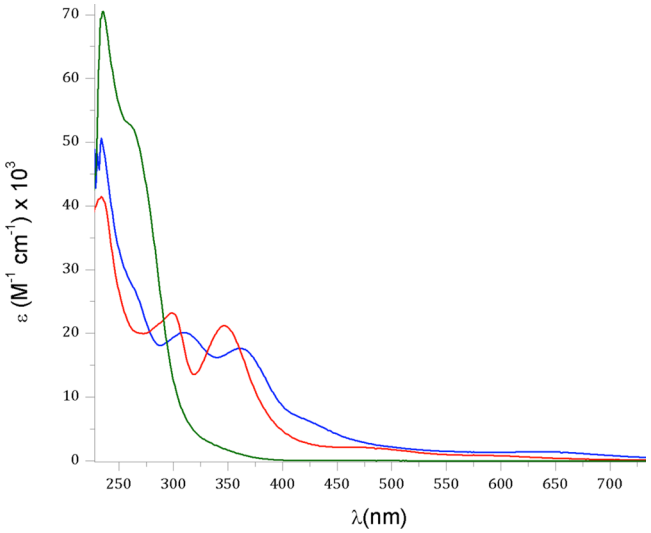

Figure 4. UV−vis spectra of **1** (blue trace), **2** (green trace), and **3** (red trace). Spectra were acquired from THF solutions ca. 0.04 mM.

to intraligand transitions; this was indirectly confirmed by comparing the UV−vis spectrum of **1** with that of the Zn^{2+} d^{10} analogue **2**, which may only exhibit ligand-based electronics transitions observed at 235 and a shoulder at 320 nm (L → L) (Figure 4, green line).

In the case of the monomeric complex **3** (Figure 4, red line), all bands are blueshifted relative to its dimeric counterpart **1**, indicative of an electronic effect of the isocyanide ligand: the bands assigned as Spσ → Ni and Spπ → Ni transitions are observed at 300 (ε = 23 128 M^{-1} cm^{-1}) and 348 nm (ε = 21 163 M^{-1} cm^{-1}), respectively.[7f] Interestingly, the shoulder at 260 nm for **1** is absent in the monomeric complex **3**, which may be associated with an interligand character of the transition; in contrast, the band assigned to the intraligand transition remains at 235 nm. All the UV−vis bands observed for **3** and **1** are very intense, reflecting a high degree of electronic delocalization between the metal orbitals and the thiolate donors, which can be directly related to a high degree of covalency of the M−S bonds as postulated by Solomon and co-workers.[15]

Reactivity Studies. Related nickel complexes are oxidized upon exposure to O_2 by intramolecular coupling of two thiyl radicals, resulting in internal disulfide formation when chelating ligands are employed.[3d,7a,b,i] Both dimeric **1** and monomeric **3** are stable to air indefinitely in THF solution; moreover, the more sterically accessible complex **3** was exposed to an atmosphere of dioxygen for several hours, without any evidence of oxidation based on UV−vis spectroscopy. Oxidation of **1** was further attempted with I_2, with no change observed after 2 d in THF solution at room temperature (r.t.); only after 48 h at 70 °C, decomposition was detected optically. Further analysis of this solution confirmed that, after being exposed to these more drastic conditions, the internal disulfide of the pincer ligand was

DOI: 10.1021/ic502547y
Inorg. Chem. 2015, 54, 619−627

formed, presumably via thiyl radicals. FAB-MS experiments allowed confirmation of the identity of the oxidation product as the intramolecular disulfide detected at m/z 768 (Supporting Information, Figure S12); colorless crystals of the disulfide (compound **1b** in Supporting Information, Figure S13) corroborated the proposed connectivity.

Another aspect of the reactivity of dimeric Ni complexes that has been evaluated is their stability toward acids. In this context, the majority of related complexes decompose by initial protonation and subsequent ligand dissociation. Thus, a THF solution of **1** was treated with 1 to 2 equiv of *p*-toluenesulfonic acid for several days without noticeable changes in the UV−vis spectra. Addition of an excess of acid gave the same result, and only after raising the temperature of the reaction mixture to 65 °C for 2 d the solution turned colorless; decomposition of **1** afforded crystals that proved to be Ni(*p*-tolyl-SO_3)$_2$·6H_2O based on preliminary diffraction data (Figure S13). The reaction of **1** with aqueous HBF_4 was also examined by UV−vis spectroscopy; a 0.04 mM THF solution of the complex was treated with 1 to 20 equiv of acid at 10 min intervals between each addition. The stability of **1** was confirmed under acidic conditions in this fashion, since no significant changes were observed in the UV−vis spectra (Supporting Information, Figure S14).

Computational Studies. The electronic properties of dimeric complex **1** and the less computationally intensive monomeric complexes **3** were analyzed by density functional theory (DFT) methods. Optimization of the molecular geometry of a simplified version of **3** was initially undertaken by replacing the isocyanide ligand for a molecule of acetonitrile in [(CH_3CN)Ni(NS_2)]; a comparative analysis was carried out on the Zn^{2+} analogue [(CH_3CN)Zn(NS_2)]. Three minima were found in the case of the Ni model complex depending on the flap conformation of the 3,5-(CF_3)$_2$$C_6H_3$ rings, all within a few kcal mol^{-1}.[16] These results suggest a dynamic behavior in solution; the optimized geometric parameters for the lowest-energy conformer are comparable to those determined crystallographically for **3**. A time-dependent DFT study was performed to calculate the electronic transitions in acetonitrile solution. The calculated spectrum of [(CH_3CN)Ni(NS_2)] is dominated by an intense band at 363 nm (f = 0.47), which was assigned to ligand-to-metal charge transfer (LMCT) from p−π (S) toward the $d_{x^2-y^2}$ (Ni) orbital (observed experimentally at 348 nm).

The two orbitals involved in the electronic transition for the analogue of **3** are shown in Figure 5; the highest occupied molecular orbital (HOMO−2) is characterized by major contribution from the sulfur lone pairs (67%), as well as some degree of participation from the π-system of the adjacent aromatic ring. Additional bands having an intensity of less than 15% are also predicted and were assigned to transitions from the thioaryl groups (452, 290 nm), π-system of acetonitrile (297, 273 nm), or aromatic rings (340, 322 nm) to the x^2-y^2 orbital. For the case of the [(CH_3CN)Zn(NS_2)] complex, the coordination geometry of the metal center is quite different, which in this case optimizes to a pseudotetrahedral geometry (see Supporting Information).

The HOMO calculated for the optimized complex **1** has also a high contribution from the sulfur atoms; in this case, the degree of participation of the nonbridging sulfur atoms is much greater than that of the sulfur bridges (Figure 6), while the lowest unoccupied molecular orbital (LUMO) is an antibonding combination of a Ni-centered orbital (d) with the S donors (p-type orbitals, see Figure 7).

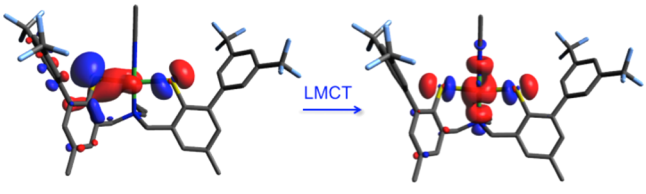

Figure 5. Isodensity contours of the orbitals (HOMO−2 and LUMO) involved in the S → Ni LMCT UV−vis band calculated for [(CH_3CN)Ni(NS_2)].

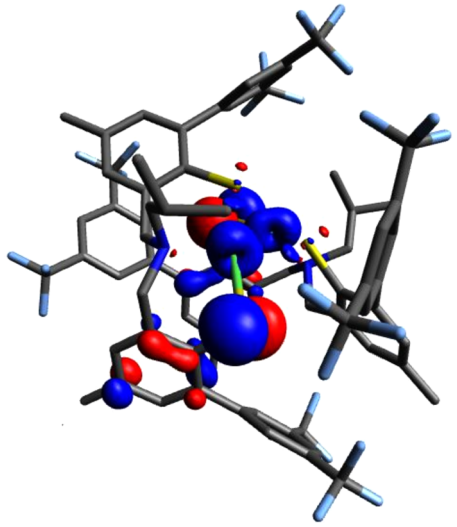

Figure 6. Isodensity contour of the HOMO calculated for **1**.

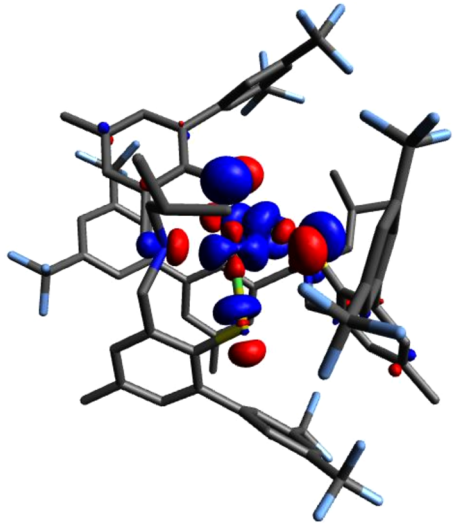

Figure 7. Isodensity contour of the LUMO calculated for **1**.

Electrochemical Studies. Electrochemical analysis of complex **1** in 0.1 M NBu_4PF_6−THF was performed under an N_2 atmosphere. Cyclic voltammograms of **1** are characterized by a reversible oxidation at $E_{1/2}$ = 0.47 V (scan rate 100 mV/s, ΔE = 160 mV, Figure 8). This process (corresponding to the anodic E^1_a and cathodic E^1_c peaks in Figure 8 and Supporting Information, Figure S17) can be interpreted as the reversible

DOI: 10.1021/ic502547y
Inorg. Chem. 2015, 54, 619−627

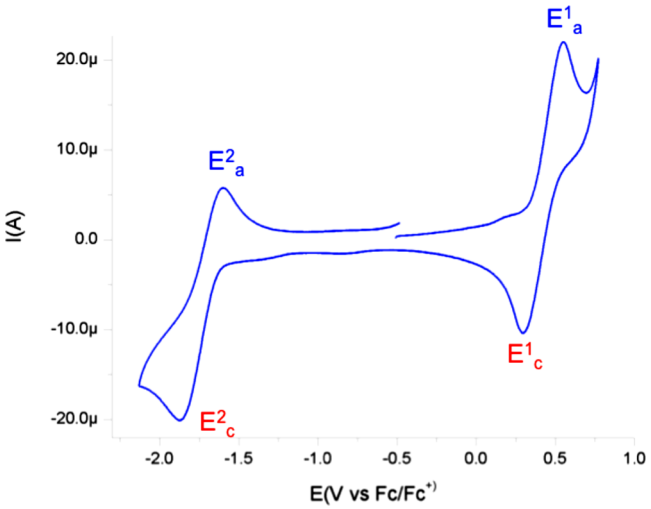

Figure 8. Anodic CV of **1** (1 mM in 0.1 M NBu_4PF_6-THF, glassy carbon electrode) at a scan rate of 0.1 V s^{-1}.

oxidation of the Ni^{2+} ions in the dimer from $Ni^{2+}Ni^{2+}$ to $Ni^{3+}Ni^{3+}$; such reversible processes can be identified as involving two electrons by comparison with the irreversible ones in monomeric complex **3**, which are characterized by currents with approximately half the value observed for **1**: the anodic peak current measured for **3** is 10.6 μA, while in the case of **1** the corresponding current measured at the same concentration is 22.0 μA (see Supporting Information, Figure S18). Scanning to negative potentials revealed the reversible reduction to $Ni^{+}Ni^{+}$ at $E_{1/2}$ = −1.66 V (ΔE = 159 mV, 20.1 μA) corresponding to the peaks E^2_a and E^2_c in Figure 8; analysis of monomeric complex **3** also shows irreversible redox waves with approximately half the intensity of the current determined for **1** (anodic peak 9.8 μA), as expected for a one-electron process (Figure S18). Noticeably, most redox potentials reported for Ni^{2+}/Ni^{3+} couples of related dimeric complexes featuring aliphatic thiolate ligands appear at lower values, although they behave irreversibly, so that only the anodic peaks are available for comparison: E^1_a = −290[7a] and −25 mV,[7c] respectively. In contrast, Millar and co-workers demonstrated that a dimeric complex with arylthiophenolate ligands, namely, $[Ni_2\{P(o\text{-}C_6H_4S)_3\}_2]^{2-}$, can be oxidized reversibly in two consecutive one-electron processes to give stable $[Ni^{3+}Ni^{2+}]$ and $[Ni^{3+}Ni^{3+}]$ species.[1b]

It is important to emphasize that in most reports regarding related dimeric Ni^{2+} complexes, electrochemical reduction to the corresponding Ni^{+} species is not observed, and only in a few instances has this been reported as an irreversible process at more negative potentials.[7] This indicates that electronic delocalization through the highly covalent Ni−S bonds and the extended aromatic system of **1**, may be a stabilizing factor to access both $Ni^{+}Ni^{+}$ and $Ni^{3+}Ni^{3+}$ complexes. The reversibility of the electrochemical processes also attests to the flexibility of the NS_2 ligand to accommodate the coordination preferences of the nickel centers from d^7 to d^9 configurations, as well as the d^{10} Zn^{2+} ions. Unambiguous assignment of the redox processes as metal-based was aided by comparison of the CVs of **1** and **2** (Supporting Information, Figure S19). The lack of easily accessible oxidation states for Zn^{2+} in complex **2** guarantees that the irreversible redox processes observed are ligand-based, in contrast with the observation of reversible processes for **1**.

Electrochemical methods are well-suited to determine the potential hydrogenase activity of Ni and Fe complexes;[17] thus, the electrocatalytic proton reduction activity of **1** was investigated in the presence HBF_4 in THF. As shown in Figure 9, sequential addition of acid from 0 to 16 equiv renders the

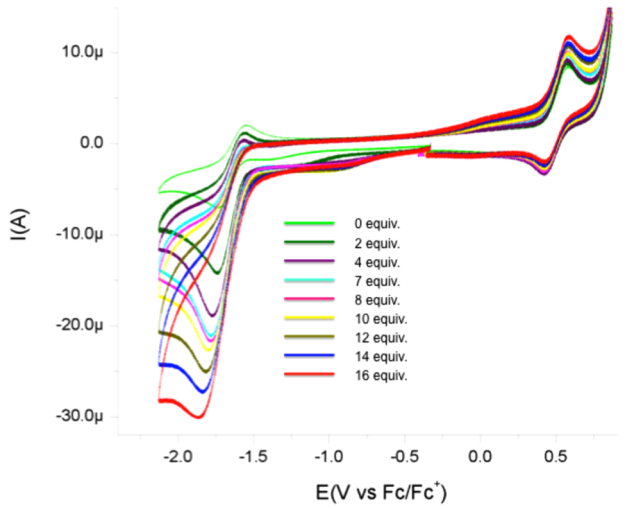

Figure 9. Cyclic voltammograms of 1 mM solutions of **1** with various amounts of HBF_4 in 0.1 M NBu_4PF_6−THF at a scan rate of 0.1 V s^{-1}.

reduction wave for the $Ni^{2+}Ni^{2+}/Ni^{+}Ni^{+}$ couple irreversible and leads to an increase in the current. This behavior is characteristic of electrocatalytic proton reduction, since direct reduction of HBF_4 at the glassy carbon electrode is negligible in this potential range (Supporting Information, Figure S20).[17] The electric current of the reduction wave at $E_{1/2}$ = −1.66 V associated with the reduction of **1** grows from −7.0 to −30 μA with increasing amounts of acid (Figure 9).

The magnitude of the peaks in the oxidative processes remains without significant changes during the proton-reduction experiments, demonstrating the stability of **1** under these conditions. Attempts to generate the putative $Ni^{+}Ni^{+}$ complex by two-electron reduction of **1** on a preparative scale for detailed examination with excess sodium amalgam were unsuccessful.

A final test was undertaken, which demonstrates the capability of **1** to also act as a catalyst for the oxidation of hydrides (Supporting Information, Figure S21). The addition of $NaBH(OAc)_3$ to THF solutions of **1** under N_2 results in an increase of the oxidative peak current (E^1_a) from 9.0 to 18 μA after addition of 4 equiv of hydride; addition of further equivalents of hydride was precluded by its low solubility in THF. These results add to the previously reported nickel-based molecular electrocatalysts for H_2 production with thiolate ligands.[18]

CONCLUSIONS

The pincer-type NS_2 ligand herein reported gives rise to robust Ni^{2+} complexes that are stable toward oxidation by dioxygen or iodine to afford the corresponding sulfinate or disulfide, respectively; this appears to be precluded by the electron-withdrawing ability of the bis(trifluoromethyl)phenyl substituents at the ortho positions relative to the sulfur donors, which also provide steric protection to the metal centers. DFT calculations indicate that the HOMO of the dinickel complex **1** has a significant contribution from the sulfur donors, but this

DOI: 10.1021/ic502547y
Inorg. Chem. 2015, 54, 619−627

Table 3. Selected Crystallographic Data for Complexes 1, 2, and 3

	1	2	3
empirical formula	$C_{72}H_{58}F_{24}N_2Ni_2S_4$	$C_{72}H_{58}F_{24}N_2S_4Zn_2$	$C_{47}H_{41}F_{12}N_3NiS_2$
formula weight	1652.86	1665.38	998.66
T [K]	132(2) K	130(2) K	133(2) K
wavelength (Å)	0.710 73 Å	0.710 73 Å	0.710 73 Å
Z	4	2	2
crystal system	monoclinic	triclinic	orthorhombic
space group	$C2/c$	$P\bar{1}$	$P21/c$
a [Å]	24.8355(18)	14.8090(10)	9.6517(9)
b [Å]	16.3722(8)	16.2035(10)	15.0585(12)
c [Å]	17.658(1)	17.0702(6)	16.2831(15)
α [deg]	90	93.146(7)	76.671(7)
β [deg]	94.566(6)	102.549(4)	98.443(5)
γ [deg]	90	114.453(6)	79.009(7)
volume [Å^3]	7157.2(7)	3591.0(4)	2260.2(3)
density (calculated)	1.534 Mg/m^3	1.541 Mg/m^3	1.467 Mg/m^3
absorption coefficient	0.749 mm^{-1}	0.890 mm^{-1}	0.609 mm^{-1}
crystal size	0.11 × 0.07 × 0.06 mm^3	0.35 × 0.30 × 0.19 mm^3	0.27 × 0.11 × 0.07 mm^3
reflections collected	7084	18152	8240
refinement method	full-matrix least-squares on F^2	full-matrix least-squares on F^2	full-matrix least-squares on F^2
goodness-of-fit on F^2	1.024	1.028	1.027
final R indices [$I > 2\sigma(I)$]	$R1$ = 0.0574, $wR2$ = 0.1234	$R1$ = 0.0505, $wR2$ = 0.1221	$R1$ = 0.0703, $wR2$ = 0.1545
R indices (all data)	$R1$ = 0.0930, $wR2$ = 0.1409	$R1$ = 0.0663, $wR2$ = 0.1350	$R1$ = 0.1167, $wR2$ = 0.1900

does not result in complex decomposition by protonation, based on the observed stability of **1** under acidic conditions by UV−vis spectroscopy. The NS_2 ligand provides electronic plasticity, as evidenced in the reversible two-electron oxidation and reduction of **1**, leading to the putative $Ni^{3+}Ni^{3+}$ and $Ni^{+}Ni^{+}$ derivatives. Pincer-type NS_2 also displays significant geometric flexibility, being able to accommodate the coordination preferences of metal ions from d^7 (Ni^{3+}) to d^{10} (Zn^{2+}) configurations. Finally, we have shown that the homodimeric complex **1** can catalyze both the electrochemical reduction of protons and the oxidation of hydrides. The combined observations place the NS_2 ligand as a robust and flexible platform for the development of metal complexes that may be employed in biologically inspired sulfur-rich systems.

EXPERIMENTAL SECTION

All synthetic operations were performed under a dry dinitrogen atmosphere in a glovebox or by conventional Schlenk techniques. THF and diethyl ether and were obtained oxygen- and water-free by distilling from sodium benzophenone under N_2 atmosphere. Reagents were purchased from commercial suppliers and used as received; the bis(*S*-arylthiocarbamate)amine ligand precursor **D** was synthesized from the corresponding *S*-formylthiocarbamate. ^{1}H and ^{13}C NMR spectra were recorded with a JEOL Eclipse 300 or a Bruker Avance DRX spectrometer at 300 and 75 MHz, respectively, using the residual protiated solvent signal or tetramethylsilane (TMS) as internal references (TMS δ = 0.00, $CHCl_3$ δ = 7.26 ppm). Electron ionization mass spectrometry (ESI MS) experiments were performed with a JEOL JMS-AX505HA spectrometer. Positive ion FAB$^+$ MS were acquired with a JEOL JMS-SX-102A mass spectrometer operated at an accelerating voltage of 10 kV from a nitrobenzyl alcohol matrix by using xenon atoms at 6 keV.

X-ray Crystallography. Data were obtained on an Oxford Diffraction Gemini A diffractometer with a CCD area detector, and the CrysAlisPro and CrysAlis RED software packages were used for data collection and data integration;[19] collected data were corrected for absorbance by using analytical numeric absorption correction using a multifaceted crystal model based on expressions upon the Laue symmetry using equivalent reflections.[20] The structures were solved using SHELXS-97[21] and refined by full-matrix least-squares on F^2 with SHELXL-97.[22] Weighted R factors, R_w, and all goodness-of-fit indicators, S, were based on F^2. The observed criterion of ($F^2 > 2\sigma F^2$) was used only for calculating the R factors. All non-hydrogen atoms were refined with anisotropic thermal parameters in the final cycles of refinement. Hydrogen atoms were placed in idealized positions, with C−H distances of 0.93 and 0.98 Å for aromatic and saturated carbon atoms, respectively. The isotropic thermal parameters of the hydrogen atoms were assigned the values of U_{iso} = 1.2 times the thermal parameters of the parent non-hydrogen atom. A summary of crystallographic data is presented in Table 3.

Computational Details. Unrestricted calculations were carried out using the Gaussian09 package.[23] The hybrid density functional method known as B3LYP was applied.[24] Effective core potentials (ECP) were used to represent the innermost electrons of the transition atoms and the basis set of valence double-z quality for associated with the pseudopotentials known as LANL2DZ.[25] The basis set for the light elements as S, C, N, and H was 6-31G*.[26] Energies in solution were taken into account by PCM calculations (acetonitrile, ε = 36.64, respectively),[27] keeping the geometry optimized for gas phase (single-point calculations). The energies calculated for the simplified version of complex **3**, namely, [(CH_3CN)Ni(NS_2)] with and without the coordinated molecule of acetonitrile, are shown in Supporting Information, Table S2; calculated bond distances and angles are shown in Supporting Information, Table S3; calculated electronic transitions are in Supporting Information, Table S4.

Electrochemical Details. Cyclic voltammetry measurements were made under N_2 in anhydrous THF with a potentiostat−galvanostat CH Instruments with a glassy carbon working electrode and a platinum wire auxiliary electrode. Potentials were recorded versus a pseudoreference electrode of AgBr(s)/Ag(wire) immersed in a 0.1 M NBu_4Br acetonitrile solution. All voltammograms were started from the current null potential (E_i = 0) and were scanned in both directions, positive and negative, and obtained at a scan rate of 0.100 and 0.200 V·s^{-1}. In agreement with IUPAC convention, the voltammogram of the ferrocinium−ferrocene (Fc^+/Fc) system was obtained to establish the values of half wave potentials ($E_{1/2}$) from the expression $E_{1/2} = (E_a + E_c)/2$. To obtain the normalized current for each complex, the measured current was divided by the exact molar concentration of the electroactive species.

DOI: 10.1021/ic502547y
Inorg. Chem. 2015, 54, 619−627

*[Ni(NS$_2$)]$_2$ (**1**).* To a solution of ^{t}BuN(STioc)$_2$ (**D**) (0.20 g, 0.22 mmol) in 50 mL of THF, a 4.1 M solution of MeONa (0.13 mL, 0.53 mmol) in ca. 5 mL of MeOH was added. The resulting yellow solution was stirred at 65 °C for 5 d. After this time, the solution appeared to have changed color to intense yellow. Then solid $NiCl_2·6H_2O$ was added, and an immediate color change to dark green was observed. The solution was evaporated to dryness under reduced pressure, and the resulting black solid was washed with MeOH and recrystallized from a 7:3 CH_3CN/diethyl ether solution to afford black crystals (0.17 g). Yield: 95%; mp > 250 °C; ^{1}H NMR (300 MHz, $CDCl_3$): δ 0.76 (d, J = 6.9 Hz, 6H, CH_3-^{i}Bu*), 1.58 (d, J = 6.9 Hz, 6H, CH_3-^{i}Bu), 2.00 (*Ar*CH_3*, 6H), 2.09 (m, 2H, −CH-^{i}Bu*, −CH-^{i}Bu), 2.41 (m, −CH_2−, 4H), 2,48 (*Ar*CH_3, 6H), 3.66 (d, J = 10.7 Hz, 2H, −CH_2−^{i}Bu*), 3.90 (d, J = 13.3 Hz, 2H, −CH_2−^{i}Bu*), 5.92, 6.62, 6.86, 7.03, 7.19, 7.51, 7.64, 7.80 ppm; ^{13}C{^{1}H} NMR (75 MHz, $CDCl_3$): δ 20.91, 21.12, 23.29, 24.90, 25.90, 65.30, 67.46, 70.06, 119.21 (m, J = 3.75,), 125.44 (s), 123.65 (q, J = 271.5, *C*F_3), 130.27 (q, J = 3.0), 130.84 (q, J = 33 Hz, Ar*C*F_3), 130.92 (q, J = 33 Hz, Ar*C*F_3), 131.55 (s), 131.70 (s), 134.97 (s), 136.94 (s), 139.42 (s), 140.20 (s), 141.71 (s), 142.56 (s), 143.51 (s), 144.85 (s) ppm; UV−vis 235 (50,638), 310 nm (26820), 361 (23530); Anal. Calcd (%) for $C_{72}H_{58}F_{24}N_2Ni_2S_4(CH_3CN)$: C, 52.47; H, 3.63; N, 2.48; found: C, 52.48; H, 2.73; N, 2.40.

*[Zn(NS$_2$)]$_2$ (**2**).* To a solution of **D** (0.28 g, 0.31 mmol) in 50 mL of THF, a 4.1 M solution of MeONa (0.22 mL, 0.92 mmol) in ca. 5 mL of MeOH was added. The resulting yellow solution was stirred at 65 °C for 5 d. After this time, the solution appeared to have changed color to intense yellow, and then solid $ZnCl_2$ was added. The solution was evaporated to dryness under reduced pressure, and the resulting colorless solid was washed with MeOH and recrystallized from a 7:3 CH_3CN/diethyl ether solution to afford colorless crystals. Yield (0.23 g) 90%; mp > 250 °C (dec 203−205 °C); ^{1}H NMR (300 MHz, $CDCl_3$): δ 1.13 (d, 6H, CH_3-^{i}Bu), 2.08 (m, 2H, −CH_2−^{i}Bu), 2.44 (s, 6H, CH_3−Ar), 2.53 (broad, 2H), 3.84 (broad, 4H, N−CH_2−Ar*), 7.11 (s, Ar), 7.24 (CH_2Cl_2), 7.40 (s, Ar), 7.74 (s, Ar), 7.81 (s, Ar) ppm; ^{13}C{^{1}H} NMR (75 MHz, $CDCl_3$): δ 21.22 (s, CH_3-^{i}Bu), 21.58 (s, CH_3−Ar), 26.48 (s, CH-^{i}Bu), 54.39 (s, CH_2−^{i}Bu), 63.58 (s, Ar−CH_2−N), 120.95 (m, Ar−CF_3), 123.34 (q, J = 270.5 Hz, CF_3), 130.25 (m, ArCF_3), 130.47 (s), 130.94 (q, J = 33 Hz, Ar−CF_3), 132.24 (s), 133.23 (s), 139.94 (s), 143.78 (s), 143.87 (s), 145.00 ppm; UV−vis 320 (shoulder) m/z (rel. Int.): 1664 (10) [M]$^+$, 329 (100); Anal. Calcd (%) for $C_{72}H_{58}F_{24}N_2Zn_2S_4$(MeOH): C, 51.63; H, 3.68; N, 1.65; found: C, 52.34; H, 3.83; N, 1.20.

*[(2,6-Me$_2$C$_6$H$_3$NC)Ni(NS$_2$)] (**3**).* To a solution of **1** (0.10 g, 0.06 mmol) in 5 mL of THF was added 2 equiv of 2,6-dimethylphenylisocyanide (2,6-$Me_2C_6H_3NC$) (0.02 g, 0.12 mmol) dissolved in 2 mL of THF; this resulted in an immediate color change from dark green to reddish-brown. The resulting solution was stirred at r.t. for 12 h to complete the reaction. Finally this solution was evaporated to dryness, and the resulting brown solid was washed with anhydrous CH_3CN and recrystallized from a 7:3 CH_3CN/diethyl ether solution. After this treatment brown crystals of **3** were obtained (0.08 g). Yield: 70%; mp > 250 °C; ^{1}H NMR (300 MHz, $CDCl_3$): δ 1.41 (d, J = 6.7 Hz, 6H, CH_3-^{i}Bu), 1.85 [s, 6H,-CH_3−Ar], 2.34 (s, 6H, −CH_3-*Ar*NC), 2.68 (d, J = 5.7 Hz, 2H, −CH_2−^{i}Bu), 2.76 (m, 1H, −CH-^{i}Bu), 3.73 (s, 4H, *N*-CH_2−*Ar*), 6.91 (d, J = 7.7 Hz, 2H, *ArS*), 7.01 (d, J = 12.5 Hz, 2H, *ArS*), 7.07 (m, 3H, *ArNC*), 7.69 (s, 2H, *ArS*), 7.99 (s, 4H, *ArS*) ppm; ^{13}C{^{1}H} NMR (75 MHz, $CDCl_3$): δ 17.90 (s), 20.94 (s), 24.23 (s), 25.72 (s), 65.49 (s), 67.62 (s), 120.45 (m, 2C), 123.69 (q, J = 270.8 Hz, 2C ArCF_3), 127.82, 129.34, 130.31 (m), 130.75 (q, J = 33 Hz, 2C), 131.43 (d, J = 3.2 Hz, 2C), 132.98 (s), 135.86 (s), 136.32 (s), 136.62 (s), 140.44 (s), 144.62 (s) ppm; UV−vis 299 nm (30940), 346 (28250); Anal. Calcd (%) for $C_{45}H_{38}F_{12}N_2NiS_2$: C, 56.44; H, 4.00; N, 2.93; found: C, 57.47; H, 2.79; N, 4.12.

■ ASSOCIATED CONTENT

Ⓢ Supporting Information

Additional electrochemical and spectroscopic data, selected X-ray crystal structural, and DFT data. This material is available free of charge via the Internet at http://pubs.acs.org.

■ AUTHOR INFORMATION

Corresponding Author

*E-mail: joseivan@unam.mx.

Notes

The authors declare no competing financial interest.

■ ACKNOWLEDGMENTS

We thank M. Orta for combustion analysis, R. P. Maya for IR spectroscopy, and L. Velasco for FAB-MS; CONACyT (Proyecto 151837, Beca 216238) and DGAPA-PAPIIT (IN210214) for financial support.

■ REFERENCES

(1) (a) Fox, S.; Wang, Y.; Silver, A.; Millar, M. *J. Am. Chem. Soc.* **1990**, *112*, 3218−3220. (b) Franolic, J. D.; Wang, W. Y.; Millar, M. *J. Am. Chem. Soc.* **1992**, *114*, 6587−6588. (c) Volbeda, A.; Charon, M.-H.; Piras, C.; Hatchikian, E. C.; Frey, M.; Fontecilla-Camps, J. C. *Nature* **1995**, *373*, 580−587. (d) Jiang, J.; Maruani, M.; Solaimanzadeh, J.; Lo, W.; Koch, S. A.; Millar, M. *Inorg. Chem.* **2009**, *48*, 6359−6361.

(2) Darnault, C.; Volbeda, A.; Kim, E. J.; Legrand, P.; Vernède, X.; Lindahl, P. A.; Fontecilla-Camps, J. C. *Nat. Struct. Biol.* **2003**, *10*, 271−279.

(3) (a) Farmer, P. J.; Verpeaux, J.-N.; Amatore, C.; Darensbourg, M. Y.; Musie, G. *J. Am. Chem. Soc.* **1994**, *116*, 9355−9356. (b) Green, K. N.; Jeffery, S. P.; Reibenspies, J. H.; Darensbourg, M. Y. *J. Am. Chem. Soc.* **2006**, *128*, 6493−6498. (c) Tard, C.; Pickett, C. J. *Chem. Rev.* **2009**, *109*, 2245−2274. (d) Ohki, Y.; Tatsumi, K. *Eur. J. Inorg. Chem.* **2011**, 973−985. (e) Simmons, T. R.; Berggren, G.; Bacchi, M.; Fontecave, M.; Artero, V. *Coord. Chem. Rev.* **2014**, *270−271*, 127−150.

(4) Harrop, T. C.; Mascharak, P. K. *Coord. Chem. Rev.* **2005**, *249*, 3007−3024.

(5) (a) Asti, M.; Cammi, R.; Cauzzi, D.; Graiff, C.; Pattacini, R.; Predieri, G.; Stercoli, A.; Tiripicchio, A. *Chem.—Eur. J.* **2005**, *11*, 3413−3419. (b) Bai, S.-Q.; Hor, T. S. A. *Chem. Commun.* **2008**, 3172−3174. (c) Klerman, Y.; Ben-Ari, E.; Diskin-Posner, Y.; Leitus, G.; Shimon, L. J. W.; Ben-David, Y.; Milstein, D. *Dalton Trans.* **2008**, 3226−3234. (d) Teratani, T.; Koizumi, T.; Yamamoto, T.; Tanaka, K.; Kanbara, T. *Dalton Trans.* **2011**, *40*, 8879−8886. (e) Wang, Q.-Q.; Begum, R. A.; Day, V. W.; Bowman-James, K. *Inorg. Chem.* **2012**, *51*, 760−762.

(6) (a) Kruger, H.-J.; Holm, R. H. *Inorg. Chem.* **1989**, *28*, 1148−1155. (b) Hahn, R.; Nakamura, A.; Tanaka, K.; Nakayama, Y. *Inorg. Chem.* **1995**, *34*, 6562−6564. (c) James, T. L.; Cai, L.; Muetterties, M. C.; Holm, R. H. *Inorg. Chem.* **1996**, *35*, 4148−4161. (d) Lee, C.-M.; Chiou, T.-W.; Chen, H.-H.; Chiang, C.-Y.; Kuo, T.-S.; Liaw, W.-F. *Inorg. Chem.* **2007**, *46*, 8913−8923. (e) Huang, D.; Deng, L.; Sun, J.; Holm, R. H. *Inorg. Chem.* **2009**, *48*, 6159−6166. (f) Warner, D. S.; Limberg, C.; Mebs, S. *Z. Anorg. Allg. Chem.* **2013**, *639*, 1577−1583.

(7) (a) Kumar, M.; Day, R. O.; Colpas, G. J.; Maroney, M. J. *J. Am. Chem. Soc.* **1989**, *111*, 5974−5976. (b) Kumar, M.; Day, R. O.; Colpas, G. J.; Maroney, M. J. *J. Am. Chem. Soc.* **1989**, *111*, 8323−8325. (c) Kruger, H.-J.; Holm, R. H. *Inorg. Chem.* **1989**, *28*, 1148−1155. (d) Colpas, G. J.; Kumar, M.; Day, R. O.; Maroney, M. J. *Inorg. Chem.* **1990**, *29*, 4779−4778. (e) Darensbourg, M. Y.; Tuntulani, T.; Reibenspies, J. H. *Inorg. Chem.* **1994**, *33*, 611−613. (f) Choudhury, S. B.; Pressler, M. A.; Mirza, S. A.; Day, R. O.; Maroney, M. J. *Inorg. Chem.* **1994**, *33*, 4831−4839. (g) Maroney, M. J.; Choudhury, S. B.; Bryngelson, P. A.; Mirza, S. A.; Sherrod, M. J. *Inorg. Chem.* **1996**, *35*, 1073−1076. (h) Kersting, B.; Siebert, D. *Inorg. Chem.* **1998**, *37*, 3820−3828. (i) Kersting, B.; Siebert, D.; Volkmer, D.; Kolm, M. J.; Janiak, C. *Inorg. Chem.* **1999**, *38*, 3871−3882.

(8) Gjoka, B.; Romano, F.; Zonta, C.; Licini, G. *Eur. J. Org. Chem.* **2011**, 5636−5640.

(9) Mondragón, A.; Monsalvo, I.; Regla, I.; Flores-Alamo, M.; Castillo, I. *Tetrahedron* **2013**, *69*, 9499−9506.

DOI: 10.1021/ic502547y
Inorg. Chem. 2015, 54, 619−627

(10) McKone, J. R.; Marinescu, S. C.; Brunschwig, B. S.; Winkler, J. R.; Gray, H. B. *Chem. Sci.* **2014**, *5*, 865−878.
(11) Aullón, G.; Ujaque, G.; Lledós, A.; Alvarez, S. *Chem.—Eur. J.* **1999**, *5*, 1391−1410.
(12) Matsumoto, T.; Ito, M.; Kotera, M.; Tatsumi, K. *Dalton Trans.* **2010**, *39*, 2995−2997.
(13) Fontecilla-Camps, J. C.; Volbeda, A.; Cavazza, C.; Nicolet, Y. *Chem. Rev.* **2007**, *107*, 4273−4303.
(14) (a) Cotton, F. A.; Zingales, F. *J. Am. Chem. Soc.* **1961**, *83*, 351−355. (b) Hou, H.; Gantzel, P. K.; Kubiak, C. P. *J. Am. Chem. Soc.* **2003**, *125*, 9564−9565. (c) Hou, H.; Gantzel, P. K.; Kubiak, C. P. *Organometallics* **2003**, *22*, 2817−2819. (d) Chang, X.; Lee, K.-E.; Jeon, S.; Kim, Y.-J.; Lee, H.-K.; Lee, S. W. *Dalton Trans.* **2005**, 3722−3732. (e) Espinet, P.; García-Orodea, E.; Miguel, A. J. *Chem. Mater.* **2004**, *16*, 551−558. (f) Boíllos, E.; Miguel, D. *Organometallics* **2004**, *23*, 2568−2572.
(15) Solomon, E. I.; Gorelsky, S. I.; Dey, A. *J. Comput. Chem.* **2006**, *27*, 1415−1428.
(16) Fandos, R.; Otero, A.; Rodríguez, A.; Terreros, P.; Aullón, G.; Alvarez, S. *Eur. J. Inorg. Chem.* **2009**, 1079−1085.
(17) (a) Ghosh, S.; Hogarth, G.; Hollingsworth, N.; Holt, K. B.; Kabirc, S. E.; Sanchez, B. E. *Chem. Commun.* **2014**, *50*, 945−947. (b) Felton, G. A. N.; Glass, R. S.; Lichtenberger, D. L.; Evans, D. H. *Inorg. Chem.* **2006**, *45*, 9181−9184. (c) Felton, G. A. N.; Vannucci, A. K.; Chen, J.; Lockett, L. T.; Okumura, N.; Petro, B. J.; Zakai, U. I.; Evans, D. H.; Glass, R. S.; Lichtenberger, D. L. *J. Am. Chem. Soc.* **2007**, *129*, 12521−12530. (d) Crouthers, D. J.; Denny, J. A.; Bethel, R. D.; Munoz, D. G.; Darensbourg, M. Y. *Organometallics* **2014**, *33*, 4747−4755. (e) Kilgore, U. J.; Roberts, J. A. S.; Pool, D. H.; Appel, A. M.; Stewart, M. P.; DuBois, M. R.; Dougherty, W. G.; Kassel, W. S.; Bullock, R. M.; DuBois, D. L. *J. Am. Chem. Soc.* **2011**, *133*, 5861−5872.
(18) (a) Zhang, W.; Hong, J.; Zheng, J.; Huang, Z.; Zhou, J.; Xu, R. *J. Am. Chem. Soc.* **2011**, *133*, 20680−20683. (b) Han, J.; Zhang, W.; Zhou, T.; Wang, X.; Xu, R. *RSC Adv.* **2012**, *2*, 8293−8296. (c) Han, Z.; Shen, L.; Brennessel, W. W.; Holland, P. L.; Eisenberg, R. *J. Am. Chem. Soc.* **2013**, *135*, 14659−14669.
(19) *CrysAlis, C. C. D. and CrysAlis, R;* Oxford Diffraction: Abingdon, U.K., 2009.
(20) Clark, R. C.; Reid, J. S. *Acta Crystallogr., Sect. A: Found. Crystallogr.* **1995**, *A51*, 887−897.
(21) Sheldrick, G. M. *SHELXS-97, Crystal Structure Solution;* University of Göttingen: Germany, 1990.
(22) Sheldrick, G. M. *SHELXL-97, Crystal Structure Refinement;* University of Göttingen: Germany, 1997.
(23) Frisch, M. J.; Trucks, G. W.; Schlegel, H. B.; Scuseria, G. E.; Robb, M. A.; Cheeseman, J. R.; Scalmani, G.; Barone, V.; Mennucci, B.; Petersson, G. A.; Nakatsuji, H.; Caricato, M.; Li, X.; Hratchian, H. P.; Izmaylov, A. F.; Bloino, J.; Zheng, G.; Sonnenberg, J. L.; Hada, M.; Ehara, M.; Toyota, K.; Fukuda, R.; Hasegawa, J.; Ishida, M.; Nakajima, T.; Honda, Y.; Kitao, O.; Nakai, H.; Vreven, T.; Montgomery, J. A.; Peralta, J. E.; Ogliaro, F.; Bearpark, M.; Heyd, J. J.; Brothers, E.; Kudin, K. N.; Staroverov, V. N.; Keith, T.; Kobayashi, R.; Normand, J.; Raghavachari, K.; Rendell, A.; Burant, J. C.; Iyengar, S. S.; Tomasi, J.; Cossi, M.; Rega, N.; J. Millam, M.; Klene, M.; Knox, J. E.; Cross, J. B.; Bakken, V.; Adamo, C.; Jaramillo, J.; Gomperts, R.; Stratmann, R. E.; Yazyev, O.; Austin, A. J.; Cammi, R.; Pomelli, C.; Ochterski, J. W.; Martin, R. L.; Morokuma, K.; Zakrzewski, V. G.; Voth, G. A.; Salvador, P.; Dannenberg, J. J.; Dapprich, S.; Daniels, A. D.; Farkas, O.; Foresman, J. B.; Ortiz, J. V.; Cioslowski, J.; Fox, D. J. *Gaussian 09 (Revision B.1)*; Gaussian, Inc.: Wallingford, CT, 2010.
(24) (a) Becke, A. D. *J. Chem. Phys.* **1993**, *98*, 5648−5652. (b) Lee, C.; Yang, W.; Parr, R. G. *Phys. Rev. B* **1988**, *37*, 785−789.
(25) Hay, P. J.; Wadt, W. R. *J. Chem. Phys.* **1985**, *82*, 299−310.
(26) (a) Hariharan, P. C.; Pople, J. A. *Theoret. Chim. Acta* **1973**, *28*, 213−222. (b) Francl, M. M.; Petro, W. J.; Hehre, W. J.; Binkley, J. S.; Gordon, M. S.; DeFrees, D. J.; Pople, J. A. *J. Chem. Phys.* **1982**, *77*, 3654−3665.
(27) (a) Tomasi, J.; Persico, M. *Chem. Rev.* **1994**, *94*, 2027−2094. (b) Amovilla, C.; Barone, V.; Cammi, R.; Cancès, E.; Cossi, M.; Mennucci, B.; Pomelli, C. S.; Tomasi, J. *Adv. Quantum Chem.* **1998**, *32*, 227−261.

DOI: 10.1021/ic502547y
Inorg. Chem. 2015, 54, 619−627